Biogeosciences Discuss., doi:10.5194/bg-2016-228, 2016
Manuscript under review for journal Biogeosciences
Published: 10 June 2016

Biogeosciences Discussions
Open Access
EGU

Linking diverse nutrient patterns to different water masses within anticyclonic eddies in the upwelling system off Peru

Yonss Saranga José, Heiner Dietze, and Andreas Oschlies
GEOMAR Helmholtz Centre for Ocean Research Kiel
Correspondence to: Yonss José (yjose@geomar.de)

Abstract. Ocean eddies can both trigger mixing (during their formation and decay) and effectively shield water encompassed from being exchanged with ambient water (throughout their life time). These antagonistic effects of eddies complicate the interpretation of synoptic snapshots as typically obtained by ship-based oceanographic measurement campaigns. Here we use a coupled physical-biogeochemical model to explore biogeochemical dynamics within anticyclonic eddies in the Eastern Tropical South Pacific ocean. The goal is to understand the diverse biogeochemical patterns that have been observed at the subsurface layers of the anticyclonic eddies in this region. Our model results suggest that the diverse subsurface nutrient patterns within eddies are associated with the presence of water masses of different origins at different depths. The water mass diversity responds to variations with depth of the circulation strength at the edge of the eddy.

1 Introduction

Satellite-based measurements have revealed strong correlations between sea surface height and ocean colour (e.g. Cipollini et al., 2001). Most of these correlations are related to nonlinear mesoscale eddies which shape a distinct biogeochemical environment that differs from ambient surrounding waters (e.g. Chelton et al., 2011). Processes proposed to shape distinctly differing environments in energetic mesoscale eddies include eddy vertical transport such as pumping during the formation and intensification (decay) of cyclonic (anticyclonic) eddies (e.g. Jenkins, 1988; Falkowski et al., 1991), and eddy/wind effects driving upwelling in anticyclonic eddies (e.g. Martin and Richards, 2001). Common to these processes is that they have been proposed to enhance near-surface vertical transport and thus increase the availability of essential nutrients in the sun-lit surface ocean (although basin-scale effects are discussed controversially e.g. Oschlies (2002); Eden and Dietze (2009)). Another trait of eddies, somewhat antagonistic, is their role in lateral transport processes. Eddies can enclose water parcels and effectively shield them from being mixed with ambient waters for months (e.g. Dietze et al., 2009). This can render the interpretation of synoptic snapshots, such as obtained by ship-based oceanographic measurement campaigns, problematic because local conditions encountered may well be the result of processes hosted hundreds of miles away in the past rather than being effected locally and contemporarily which, in turn, can obscure causal relationships.

This study sets out to investigate, if and to what extend standing stocks of biogeochemically relevant species are decoupled from local contemporary processes in eddies in the Eastern Tropical Pacific (*ETSP*). The region is known for oxygen-deprived waters at intermediate depth that host anoxic biogeochemical cycling of organic matter such as denitrification and anammox

Biogeosciences Discuss., doi:10.5194/bg-2016-228, 2016
Manuscript under review for journal Biogeosciences
Published: 10 June 2016

– both of which are key to setting the global inventory of bioavailable nitrogen that is essential for phytoplankton growth. A recent survey in the *ETSP* oxygen minimum zone (*OMZ*) revealed strong correlations between mesoscale eddies and subsurface nutrients (Altabet et al., 2012; Stramma et al. , 2013). Specifically two anticyclonic eddies were identified associated with both low and high nitrate concentration in their centre. As concerns the low-nitrate eddy, Stramma et al. (2013) corroborated the suggestion put forward by Altabet et al. (2012) that the nitrate deficit is caused by local denitrification and/or DNRA. As for the high-nitrate eddy, the authors speculated that the nutrient anomaly is related to the initial concentration at the time and place of the eddy formation. We speculate that a more comprehensive analysis of eddies in the region, which explicitly considers their life history, will provide new insights. To this end we will apply a coupled, eddy-resolving ocean circulation biogeochemical model of the *ETSP*. Eddies similar to those observed by Altabet et al. (2012) and Stramma et al. (2013) will be analysed. The focus is on nutrient dynamics and water mass properties within the eddies throughout their lifetime.

2 Methods

We employ the Regional Oceanic Model System (*ROMS*, Shchepetkin and McWilliams (2005)) to simulate the dynamics of the *ETSP* ocean. This free-surface and terrain-following vertical coordinates model (Shchepetkin and McWilliams, 2005) allows to allocate high resolution in the surface and coastal regions, that are crucial for the biogeochemical processes. The *ROMS* model is coupled with *BioEBUS* (**Bio**geochemical model for the **E**astern **B**oundary **U**pwelling **S**ystems) to simulate the first trophic levels of the food web and the biogeochemical dynamics. A complete description and validation of the *BioEBUS* is presented in Gutknecht et al. (2013). The first trophic levels of *BioEBUS* model consist on small (flagellated and microzooplankton) and large (diatoms and mesozooplankton) organisms. The flagellates differ from the diatoms by their adaptation to low nutrients and stratified conditions, as well as their better assimilation efficiency for nutrients. The *BioEBUS* model is a nitrogen-based model that accounts for denitrification, nitrification and anammox. Nitrate, nitrite and ammonium are prognostic variables. The model has been developed to resolve the biogeochemical processes of the eastern boundary upwelling systems under oxic, hypoxic and suboxic conditions.

We employ a 2 ways-nesting procedure (Debreu et al., 2012) to embed a small regional domain within a large-scale domain. The large domain, extends from 69°W to about 120°W in longitude and from 18°N to 40°S in latitude. It features a horizontal resolution of $\frac{1}{4}^{\circ}$. The embedded domain features a high resolution grid of $\frac{1}{12}^{\circ}$ and extends from around 5°N to 31°S in latitude and around 69°W to 102°W in longitude. Both domains feature 32 vertical levels. The underlying topography of both large-scale and regional domain is derived from the GEBCO at 1 minute resolution (IOC, IHO and BODC , 2003).

The *ROMS* model is forced at the surface with monthly climatological fluxes of heat and fresh water from *COADS* (Worley et al., 2005). Wind fields are from *QuikSCAT* (Liu et al., 1998). At its boundaries, the large scale domain is nudged toward monthly climatological (1990-2010) *SODA* reanalysis (Carton and Giese, 2008). The *BioEBUS* model is constrained at the boundary with monthly climatological nitrate and oxygen from *CARS* (Ridgway et al., 2002). The phytoplankton boundary condition is derived from the monthly climatological surface chlorophyll data from *SeaWiFs* (O'Reilly et al., 1998). This surface chlorophyll data is then extrapolated vertically following the Morel and Berthon (1989) parameterization (Gutknecht

Biogeosciences Discuss., doi:10.5194/bg-2016-228, 2016
Manuscript under review for journal Biogeosciences
Published: 10 June 2016

et al., 2013). The lateral boundary conditions for zooplankton forcing is based on an analytical function, depending on the vertical distribution of chlorophyll (Gutknecht et al., 2013). For the analysis in this paper, physical and biogeochemical dynamics of the *ETSP* are averaged over 5 years of simulation, after a spin-up time of 25 climatological years

2.1 Model evaluation

Figure 1 shows the simulated physical dynamics of the *ETSP* along with respective observations. At the surface, the simulated surface eddy kinetic energy (*EKE*) is increased along the coast (Fig. 1-a). This pattern is in agreement with the observed surface *EKE* derived from *AVISO* altimetry product (http://www.aviso.altimetry.fr/duacs/) over a period from 1993 to 2012 (Fig. 1-b). The surface currents, namely the Peru Oceanic Current in the open ocean and the Peru Coastal Current (PCC), are visible propagating north-westward, contributing to the westward South Equatorial Current (*SEC*, contours in Fig. 1-a,b). Along the coast, the model solution shows a southward flow at the subsurface layers (Fig. 1-c,e), in agreement with the observations (Fig. 1-d,f, Chaigneau et al. (2013)). In the north, the southward Equator - Peru Coastal Current (*EPCC*) is intensified in the upper 150 m depth (Fig. 1-c,d). This alongshore current is still present 150 km offshore, with velocities around 5 $\mathrm{cm\,s^{-1}}$. Further south, the simulated subsurface Peru-Chile Under Current (*PCUC*, Fig. 1-e) is deeper (between 50 and 250 m depth) and more intensified than the *EPCC* (Fig. 1-c,d). An equatorward flow inshore is also visible in the simulated dynamics (Fig. 1-e) and is consistent with the observations presented by Thomsen et al. (2015). This equatorward flow is related to the northward PCC observed along the coast (Smith , 1986; Thomsen et al. , 2015). The equatorward current is observed between the surface down to about 60 m depth. Despite the good representation of the alongshore currents, the model underestimates the intensity of both the *EPCC* and the *PCUC*. This might be related to the low resolution of the boundary conditions used in this configuration.

Figure 2 present the spatial distribution of simulated and observed biogeochemical dynamics. The simulated (Fig. 2-a) as well as the remotely sensed (*MODIS*) surface chlorophyll (Fig. 2-b, Zibordi et al. (2006)) show high concentrations along the coast. The highest values are observed along the Peru upwelling region (between 5°S and 16°S), related to the upward transport of deep nutrient-rich waters (Chavez et al., 2008). The simulated oxygen content at 400 m depth is relatively high around the equator, which is consistent with the observed dynamics (Fig. 2-c,d). Vertically, the oxygen distribution shows less oxygenated waters at intermediate depths (Fig. 3-a), in-line with observations (Czeschel et al., 2011, 2015). However, the thickness of these oxygen-depleted waters is thinner in the model solution. The simulated nitrate concentrations closely match the observed vertical nitrate distribution, in spite of the fact that the deeper nitrate is underestimated in the simulated dynamics (Fig. 3-b). The vertical structure of nitrite concentrations shows high values inshore and in the subsurface layer (Fig. 2-c). This is in agreement with the observations (Fig. 3-f). However, the magnitude of simulated nitrite is lower compared to the observations. This discrepancy can be related to the absence of sediment dynamics in this model configuration. The ammonium released from the sediments in this region (Bohlen et al., 2012) might be reduced into nitrite during nitrification processes, enhancing the water column nitrite concentrations. Sedimentary dynamics might also influence both oxygen and nitrate water column distribution. While there is no flux of matter through the bottom in the current model version, a subsequent modelling study will investigate the coupling of benthic processes.

Biogeosciences Discuss., doi:10.5194/bg-2016-228, 2016
Manuscript under review for journal Biogeosciences
Published: 10 June 2016

2.2 The eddy identification

To analyse the source of nutrients within anticyclonic eddies, we identified two anticyclonic eddies types in the simulated physical-biogeochemical dynamics (Fig. 4 and Fig. 5). Note that the patterns of the selected eddies are consistent with the *in situ* observed biogeochemical patterns presented by Stramma et al. (2013). Once identified (from now on called identification instant), we tracked the eddies backward in time and analysed their life history. An analysis of the eddy's evolution into the future after the identification instant is also presented in this paper, allowing for a more complete description of the eddy life history.

The determination of eddy shape is defined based on combination of closed contours of the sea surface height (SSH) anomalies and the Okubo-Weiss parameter (José et al. , 2014; Halo et al. , 2014). The first method identifies the closed contour of SSH (Chelton et al., 2011), according to the second, the eddy shape is defined as a connected region where the vorticity dominates strain, i.e where the Okubo-Weiss parameter is negative (Chelton et al., 2007). Combining the closed contours and the negative Okubo–Weiss parameter allows to reduce uncertainties associated with either method (Halo et al. , 2014).

2.2.1 Subsurface low nitrate and high nitrite eddy (A_{sim})

Simulated eddy A_{sim} is located at the southern part of the Peruvian coast, between 13°S and 15.5°S in latitude and 76°W and 78°W in longitude (Fig. 4-a). This eddy presents oxygen-depleted intermediate waters in its centre, with values below 20 $\mu\,\mathrm{mol\,l^{-1}}$ (Fig. 4-b). Nitrate-reduced waters also appear in the centre of the eddy (Fig. 4-c), apparently indicative of on-going denitrification within the structure, as suggested in previous studies (Altabet et al., 2012; Stramma et al. , 2013). At the edge of the structure, the nitrate concentration is higher, suggesting an exchange with surrounding waters (Fig. 4-c). In contrast, the nitrite concentration is higher in the centre and low at the edge (Fig. 4-d).

The eddy A_{sim} is intensified from the surface down to 500 m depth, with maximum surface velocity above 30 $\mathrm{cm\,s^{-1}}$ (Fig. 4-e,f). At the identification instant, this eddy shows an asymmetric velocity distribution, with weaker strength of the westward component than the eastward component (Fig. 4-f). Temperature and salinity show depressed isolines in the centre of the eddy (Fig. 4-g,h), typical of a mode-water anticyclonic eddy. The mode-water eddies are suggested to trap and isolate water from the surrounding environment.

2.2.2 Subsurface high nitrate and nitrite eddy (B_{sim})

The simulated eddy B_{sim} is an open ocean eddy, located between 12°S and 14.5°S in latitude and 84°W and 88°W in longitude (Fig. 5-a). This eddy also presents extremely low oxygen concentrations at intermediate depths in its center (Fig. 5-b). The oxygen-depleted waters are enclosed by well-oxygenated waters from the eddy's edge (Fig. 5-b). The eddy B_{sim} shows increased subsurface nitrate concentrations in the centre and slightly reduced nitrate concentrations along the edge (Fig. 5-c). The vertical structure of nitrite concentrations show isolated subsurface high-nitrite waters in the centre of the eddy (Fig. 5-d).

Biogeosciences Discuss., doi:10.5194/bg-2016-228, 2016
Manuscript under review for journal Biogeosciences
Published: 10 June 2016

At the identification instant, also the flows around the eddy B_{sim} reveals significant asymmetries. Minimum velocities are present in the eastward (surface) and westward (subsurface) flow components. This open ocean eddy shows elevated temperature and salinity in the centre, characteristics of a mode-water anticyclonic eddy (Fig. 5-g,h).

3 Result and discussion

3.1 Local biogeochemical dynamics within the eddies

In order to assess the contribution of local biogeochemical dynamics to nutrient variations within the eddy, we analyse here the production and reduction rates of each nutrient at the identification instant. Figure 6 shows the vertical distribution of reduction and production rates of nitrate (Fig. 6-a-b) and nitrite (Fig. 6-d-e) within the eddy A_{sim}. The net production (production - reduction) is also presented, for both nitrate (Fig. 6-c) and nitrite(Fig. 6-f). Below the surface of the eddy A_{sim},, the nitrate reduction via denitrification (Fig. 6-a) is lower when compared to the production (Fig. 6-b), showing a net nitrate increase due to biogeochemical processes within the eddy (Fig. 6-c). Regarding the nitrite dynamics, production and reduction rates show similar patterns. Below the surface, the nitrite reduction is slightly higher than the production (Fig. 6-d-f), suggesting that local biogeochemical processes can not explain the accumulation of high nitrite values in the centre of this eddy (Fig. 4-d). Figure 7 shows the time evolution of production and reduction rates of both nutrients (nitrate and nitrite) within the eddy A_{sim}. For comparison, nutrient concentrations during this period are also presented. Both reduction and production of nutrients within the eddy do not show any trend that could explain the reduced nitrate in the centre of the eddy. The nitrate production is higher than the reduction, showing a net increase of nitrate due to biogeochemical processes within the eddy A_{sim} (Fig. 7-a). But the magnitude of the locally produced nitrate is low compared to total changes in nitrate concentration during the eddy propagation. Local nitrite reduction is higher than local production during the eddy propagation (Fig. 7-b). The pattern of local net nitrite production is not correlated with the total changes in nitrite concentrations. These results show that the low nitrate (high nitrite) within the eddy A_{sim} is not primarily controlled by local biogeochemical dynamics within the eddy A_{sim}.

In the eddy B_{sim}, the vertical structure of production and reduction rates of nitrate show a net nitrate production in the upper layers as well as at the edge of the eddy (Fig. 8-a,b,c). The local nitrate dynamics during the propagation of eddy B_{sim} show elevated nitrate production in comparison to the reduction (Fig. 9-a). Although the net increase, the pattern as well as the magnitude of the locally produced nitrate do not match with changes in total nitrate concentrations. The vertical structure of nitrite production also reflects elevated values in the upper surface layer (Fig. 8-d,e,f). Below the surface, nitrite reduction dominates the local dynamics, with no difference between the centre and the edge of the eddy. The nitrite dynamics during the eddy propagation show a local dominance of nitrite production within the eddy, which is inconsistent with the temporal variations of nitrite concentrations (Fig. 9-b).

The inconsistency between local biogeochemical sources and sinks of nitrate and nitrite and total temporal changes of those nutrients within the eddies suggest that the biogeochemical dynamics do not exert the dominant control on the variation in nutrient concentrations.

Biogeosciences Discuss., doi:10.5194/bg-2016-228, 2016
Manuscript under review for journal Biogeosciences
Published: 10 June 2016

3.2 Water mass properties within the eddies

One important aspect of eddies is their capacity to entrain surrounding waters during their propagation (Dietze et al., 2009; José et al. , 2014). These dynamics have been pointed to stimulate the productivity within anticyclonic eddies (Dietze et al., 2009; José et al. , 2014). In the eastern tropical ocean, eddies have been observed to carry low-oxygen waters out of the core region of the *OMZ* (Stramma et al. , 2014; Karstensen et al., 2015). This make the analysis of the eddy life history essential for understanding the dynamics in the eddy interior. To resume on the origin of water masses present in the selected eddies, we analyse the water mass properties within the structure and compared it with the surrounding environment at different instants of the eddy's lifetime (Fig. 10 and Fig. 11). Figure 10 presents the water mass properties within the eddy A_{sim}. It shows relatively warmer and saltier surface waters within the eddy compared to the surrounding shelf waters (Fig. 10-a-b). When the eddy A_{sim} was formed, the surface waters were even warmer and saltier, characteristic of offshore waters. During the propagation of eddy A_{sim}, the water masses within the structure are mixed with colder and fresher coastal waters, resulting in heat and salt loss (Fig. 10-c). However, water masses within the eddy are still dominantly from the offshore region. The offshore region is a nitrate-poor environment, with minimum concentrations below 5 $\mu\,\mathrm{mol\,l^{-1}}$ (Fig. 10-d). At 100 m depth, water masses within the eddy are relatively fresher and cooler and do not match those of the offshore environment (Fig. 10-e-g). Although roughly associated with shelf waters, the water masses within the eddy at this depth are saltier and warmer than those from the shelf. At eddy formation, the water masses within the eddy were even warmer and saltier, suggesting a dominance of offshore waters within the structure. During the eddy propagation, the fresher and colder shelf waters entered the eddy interior, resulting in a cooling and freshening of the water masses within the structure. As a result, shelf waters carrying high nitrate concentrations dominate the eddy interior (Fig. 10-e-g). Further down (at 250 m depth), warmer and saltier shelf waters dominate the properties within the eddy A_{sim} (Fig. 10-1,j). At this depth, water properties are slightly modified during the eddy propagation (Fig. 10-k). Shelf waters, which have lower nitrate concentrations compared to the offshore environment, are kept in the eddy centre and advected during the eddy propagation (Fig. 10-l).

The water mass properties within the eddy B_{sim} are presented in Figure 11. Located far from the shelf region, the water masses within the eddy B_{sim} are distinct from those from the shelf. At the surface, relatively cooler and saltier waters occupy the eddy interior (Fig. 11-a,b). These waters match those from the south, which are propagated northward by the eddy. During the eddy propagation, mixing with the warmer northern waters increases the eddy surface water temperature (Fig. 11-c). This intrusion of warmer waters can also be seen from the limb of warmer waters at the north-western side of the eddy (Fig. 11-b). These dynamics are also visible at 100 m depth (Fig. 11-e,f,g). At this depth, warmer and saltier southern waters enters the eddy interior and are mixed with the fresher and colder northern waters. However, only relatively small changes occurs during the eddy propagation (Fig. 11-g). Consequently, nitrate-poor southern waters are trapped within the eddy (Fig. 11-h). The weak water mass exchange with surrounding waters during the eddy propagation is also visible at 250 m depth (Fig. 11-k). At this depth, warmer and saltier northern waters dominates the eddy interior (Fig. 11-i,j). These waters are rich in nitrate (Fig. 11-k), explaining the elevated nitrate in Figure 5. The weak water mass exchange between the eddy and environment (Fig. 11-g,k)

Biogeosciences Discuss., doi:10.5194/bg-2016-228, 2016
Manuscript under review for journal Biogeosciences
Published: 10 June 2016

combined with the meridional temperature and salinity gradient (Fig. 11-e,f,i,j), suggests that the eddy B_{sim} driven mixing is not strong enough to overcome the thermohaline front.

4 Conclusions

Recent studies have suggested an important role of eddy dynamics in controlling nutrient distribution and biogeochemical dynamics in the *OMZ* of the *ETSP* (Altabet et al., 2012; Stramma et al. , 2013). Eddy features have been suggested to induce changes in the subsurface nutrient dynamics, which may lead to N-loss, likely to induce changes in productivity and subsequently the oxygen distribution. Using a coupled physical-biogeochemical model, we investigate the nutrient dynamics within the eddy interior. Two anticyclonic eddies, based on their subsurface nitrate and nitrite patterns, were selected from the simulated dynamics and analysed. Results show a decoupling between local nitrate reduction (nitrite production) via biogeochemical processes and total changes in nitrate (nitrite) within the eddy. Analysis of water mass properties show that the nutrient signature within the selected structures is related to the presence of water masses from different origins. This variability is attributed to the variations with depth of the strength of the eddy rotational speed in the edge of the structure. Weak eddy rotation at the edge of an eddy allows an injection of either shelf and/or offshore waters, depending on the direction of the weakened flow. Our findings suggest that the biogeochemical patterns at the subsurface layer of the observed eddies in the *ETSP* are likely to be related to the presence of water masses from different origin, which are trapped and are retained within the structure.

Acknowledgements. This work is financially supported by the Deutsche Forschungsgemeinschaft (DFG), under the Sonderforschungsbereich 754 “Climate-Biogeochemistry Interactions in the Tropical Ocean” project (www.sfb754.de). Simulations were performed using the computing facilities of the Christian-Albrechts-Universität zu Kiel (NESH) and Norddeutscher Verbund zur Förderung des Hoch- und Höchstleistungsrechnens - HLRN. *In situ* circulation data were provided by the Instituto del Mar del Perú (IMARPE). We are grateful to A. Chaigneau for providing the in situ observations. Nutrient and oxygen *in situ* data were obtained from the German Collaborative Research Center (SFB 754).

Biogeosciences Discuss., doi:10.5194/bg-2016-228, 2016
Manuscript under review for journal Biogeosciences
Published: 10 June 2016

References

Altabet M. A, E. Ryabenko, L. Stramma, D. W. R. Wallace, M. Frank, P. Grasse, and G. Lavik, An eddy-stimulated hotspot for fixed nitrogen-loss from the Peru oxygen minimum zone, *Biogeosciences*, *9*, 1-120, doi:10.5194/bg-9-1-2012, 2012.

Bohlen L., A. W. Dale, and K. Wallmann, Simple transfer functions for calculating benthic fixed nitrogen losses and C:N:P regeneration ratios in global biogeochemical models, *GLOBAL BIOGEOCHEMICAL CYCLES*, *26*, 1-16, doi: 10.1029/2011GB004198, 2012.

Carton J. A. and B. S. Giese, A Reanalysis of Ocean Climate Using Simple Ocean Data Assimilation (SODA), *American Meteorological Society*, *136*, 2999 - 3017, doi:10.1175/2007MWR1978.1, 2008.

Chaigneau, A., A. Gizolme and C. Grados, Mesoscale eddies off Peru in altimeter records: Identification algorithms and eddy spatio-temporal patterns, *Progress in Oceanography*, *79*, 106,Äì119, doi:10.1016/j.pocean.2008.10.013, 2008.

Chaigneau, A., N. Dominguez, G. Eldin, L. Vasquez, R. Flores, C. Grados and V. Echevin, Near-coastal circulation in the Northern Humboldt Current System from shipboard ADCP data, *Journal of Geophysical research*, *118*, 1-16, doi:10.1002/jgrc.20328, 2013.

Chavez F. P., A. Bertrand, R. Guevara-Carrasco, P. Soler and J. Csirke, The northern Humboldt Current System: Brief history, present status and a view towards the future, *Progress in Oceanography*, *79*, 95-105, doi:10.1016/j.pocean.2008.10.012, 2008.

Chavez F. P. and M. Messié, A comparison of Eastern Boundary Upwelling Ecosystems, *Progress in Oceanography*, *83*, 80-96, doi:10.1016/j.pocean.2009.07.032, 2009.

Chelton, D. B., M. G. Schlax, R. M. Samelson and R. A. de Szoeke, Global observations of large oceanic eddies, *Geophysical Research Letters*, *34*, 1-5, doi:10.1029/2007GL030812, 2007.

Chelton, D. B., P. Gaube, M. G. Schlax, J.J. Early and R. M. Samelson, The Influence of Nonlinear Mesoscale Eddies on Near-Surface Oceanic Chlorophyll, *Science*, *334*, 328-332, doi:10.1126/science.1208897, 2011.

Chelton, M. G. Schlax and R. M. Samelson, Global observations of nonlinear mesoscale eddies, *Progress in Oceanography*, *91*, 167-216, doi:10.1016/j.pocean.2011.01.002, 2011.

Cipollini, P., D. Cromwell, P. G. Challenor and S. Raffaglio, Rossby waves detected in global ocean colour data, *Geophysical Research Letters*, *28*, 2, 323-326, 2001.

Colas, F., J. C. McWilliams, X. Capet and J. Kurian, Heat balance and eddies in the Peru-Chile current system, *Climate Dynamics*, *39*, 509-529, 2012.

Czeschel, R., L. Stramma, F. U. Schwarzkopf, B. S. Giese, A. Funk, and J. Karstensen, Middepth circulation of the eastern tropical South Pacific and its link to the oxygen minimum zone, *Journal of Geophysical research*, *116*, 1-13, doi:10.1029/2010JC006565, 2011.

Czeschel, R., L. Stramma, R. A. Weller, and T. Fischer, Circulation, eddies, oxygen, and nutrient changes in the eastern tropical South Pacific Ocean, *Ocean Science*, *11*, 455-470, doi:10.5194/os-11-455-2015, 2015.

Debreu L., P. Marchesiello, P. Penven and G. Cambon, Two-way nesting in split-explicit ocean models: algorithms, implementation and validation, *Ocean modelling*, *49-50*, 1-21, 2012.

Dietze, H., Matear, R. and T. Moore, Nutrient supply to anticyclonic meso-scale eddies off western Austrailia estimated with artificial tracers released in a circulation model, *Deep-Sea Reserach I*, *56*, 1440-1448, doi:10.1016/j.dsr.2009.04.012, 2009.

Donohue K. A., E. Firing, G. D. Rowe, A.Ishida and H. Mitsudera, Equatorial Pacific Subsurface Countercurrents: A Model–Data Comparison in Stream Coordinates*, *Journal of Physical Oceanography*, *32*, 1252-1264, 2002.

Ducet N., P. Y. Le Traon and R. Reverdin, Global high-resolution mapping of ocean circulation from TOPEX/Poseidon and ERS-1 and -2, *Journal of Geophysical research*, *105*, 19477-19498, doi:10.1029/2010JC006565, 2000.

Echevin, V., A. Albert, M. Levy, M. Graco, O. Aumont, A. Piétri and G. Garric, Intraseasonal variability of nearshore productivity in the Northern Humboldt Current System: The role of coastal trapped waves, *Continental Shelf Research*, *73*, 14-30, doi:10.1016/j.csr.2013.11.015, 2014.

Eden, C. and H. Dietze, Effects of mesoscale eddy/wind interaction on biological new production and eddy kinetic energy, *Journal of Geophysical Research*, *114*, C05023, doi:10.1029/2008JC005129, 2009.

Falkowski, P., D. Ziemann, Z. Kolber and P. Bienfang, Role of eddy pumping in enhancing primary production in the ocean, *Nature*, *352*, 55-58, 1991.

Gutknecht E., I. Dadou, B. Le Vu, G. Cambon, J. Sudre, V. Garçon, E. Machu, T. Rixen, A. Kock, A. Flohr, A. Paulmier, and G. Lavik, Coupled physical/biogeochemical modeling including O2-dependent processes in the Eastern Boundary Upwelling Systems: application in the Benguela, *Biogeosciences*, **10**, 3559-3591, 2013.

Gruber N., Lachkar Z., Frenzel H., Marchesiello P., M´unnich M., McWilliams J. C., Nagai T. and Plattner G. K., Eddy-induced reduction of biological production in eastern boundary upwelling systems, *Nature Geoscience*, **4**, 787-792, doi:10.1038/NGEO1273, 2011.

Halo I., B. Backeberg, P. Penven, C. Reason, I. Ansorge and J. Ulgren, Eddy properties in the Mozambique Channel: A comparison between satellite altimetry and Ocean Circulation models", *Deep Sea Research II*, *100*, 119-135, doi:10.1016/j.dsr2.2013.10.015, 2014

IOC, IHO and BODC, Centenary Edition of the GEBCO Digital Atlas, published on CD-ROM on behalf of the Intergovernmental Oceanographic Commission and the International Hydrographic Organization as part of the General Bathymetric Chart of the Oceans, British Oceanographic Data Centre, Liverpool, 2003.

Jenkins, W., Nitrate flux into the euphotic zone near Bermuda, *Nature*, *331*, 521-523, 1988.

José Y. S., O. Aumont, E. Machu, P. Penven, C. L. Moloney and O. Maury, Influence of mesoscale eddies on biological production in the Mozambique Channel: Several contrasted examples from a coupled ocean-biogeochemistry Model, *Deep Sea Research II*, *100*, 79-93, doi:10.1016/j.dsr2.2013.10.018, 2014.

Karstensen J., L. Stramma and M. Visbeck, Oxygen minimum zones in the eastern tropical Atlantic and Pacific oceans, *Progress in Oceanography*, *77*, 331-350, doi:10.1016/j.pocean.2007.05.009, 2008.

Karstensen J., B. Fiedler, F. Schütte, P. Brandt, A. Körtzinger, G. Fischer, R. Zantopp, J. Hahn, M. Visbeck and D. Wallace, Open ocean dead zones in the tropical North Atlantic Ocean, *Biogeosciences*, *12*, 2597-2605, doi:10.5194/bg-12-2597-2015, 2015.

Liu W. T., W. Tang and P. S. Polito, NASA scatterometer provides global ocean-surface wind fields with more structures than numerical weather prediction, *Geophysical research letters*, *25*, 761-764, 1998.

A. Mahadevan, Eddy effects on biogeochemistry,1-2, doi:10.1038/nature13048, 2014.

Martin A. and K. Richards, Mechanism for vertical nutrient transport within a North Atlantic mesoscale eddy, *Deep Sea Research, Part II*, *48*, 757-773, 2001.

Montes I., F. Colas, X. Capet and W. Schneider, On the pathways of the equatorial subsurface currents in the eastern equatorial Pacific and their contributions to the Peru - Chile Undercurrent, *Journal of Geophysical research*, *115*, 1-16, doi:10.1029/2009JC005710, 2010.

Montes I., B. Dewitte, E. Gutknecht, A. Paulmier, I. Dadou, A. Oschlies and V. Garçon, High-resolution modeling of the Eastern Tropical Pacific oxygen minimum zone: Sensitivity to the tropical oceanic circulation, *Journal of Geophysical research*, *119*, 1-18, 2014.

Morel A. and J. F. Berthon, Surface pigments, algal biomass profiles, and potential production of the euphotic layer: Relationships reinvestigated in view of remote-sensing applications, *Limnology. Oceanography*, *34*, 1545-1562, 1989.

Oschlies A., Can eddies make ocean deserts bloom? *Global Biogeochemical Cycles*, *16*, 4, 1106, doi:10.1029/2001GB001830, 2002.

Penven, P., V. Echevin, J. Pasapera, F. Colas, and J. Tam, Average circulation, seasonal cycle, and mesoscale dynamics of the Peru Current System: A modeling approach, *Journal of Geophysical research*, *110*, 1-21, doi:10.1029/2005JC002945, 2005.

O'Reilly J. E., S. Maritorena, B. G. Mitchell, D. A. Siegel, K. L. Carder, S. A. Garver, M. Kahru and C. McClain, Ocean color chlorophyll algorithms for SeaWiFS, *Journal of Geophysical research*, *103*, 24937-24953, 1998.

Ridgway K. R., J. R. Dunn and J. L. Wilkin, Ocean interpolation by four-dimensional weighted least Squares-Application to the waters around Australasia, *Journal of Atmospheric and Oceanic Technology*, *19*, 1357-1375, 2002.

Silva, N., N. Rojas and A. Fedele, Water masses in the Humboldt Current System: Properties, distribution, and the nitrate deficit as a chemical water mass tracer for Equatorial Subsurface Water off Chile, *Deep-Sea Research II*, *56*, 1004 - 1020, doi:10.1016/j.dsr2.2008.12.013, 2009.

Smith R. L., Peru Coastal Currents During El Niño:1976 and 1982, *Science*, *221*, 1397-1399, doi: 100.1126/science.221.4618.1397, 1983.

Stramma, L., G. C. Johnson, E. Firing and S. Schmidtko, Eastern Pacific oxygen minimum zones: Supply paths and multidecadal changes, *Journal of Geophysical research*, *115*, 1-12, doi:10.1029/2009JC005976, 2010.

Stramma L., H. W. Bange, R. Czeschel, A. Lorenzo and M. Frank, On the role of mesoscale eddies for the biological productivity and biogeochemistry in the eastern tropical Pacific Ocean off Peru, *Biogeosciences*, *10*, 7293-7306, doi: 10.5194/bg-10-7293-2013, 2013.

Stramma L., R. A. Weller, R. Czeschel and S. Bigorre, Eddies and an extreme water mass anomaly observed in the eastern south Pacific at the Stratus mooring, *Journal of Geophysical Research Oceans*, *119*, 1068-1083, doi:10.1002/2013JC009470, 2014.

Shchepetkin A. F. and J. C. McWilliams, The regional oceanic modeling system (ROMS): a split-explicit, free-surface, topography-following-coordinate oceanic model, *Ocean modelling*, *19*, 347-404, 2005.

T. Kanzow, G. Krahmann, R. J. Greatbatch, M. Dengler and G. Lavik, The formation of a subsurface anticyclonic eddy in the Peru-Chile Undercurrent and its impact on the near-coastal salinity, oxygen, and nutrient distributions, *Journal of Geophysical Research Oceans*, *120*, doi: 10.1002/2015JC010878, 2015.

Zibordi G., F. Meĺin and J. F. Berthon, Comparison of SeaWiFS, MODIS and MERIS radiometric products at a coastal site, *Geophysical research letters*, *33*, 1 - 4, doi:10.1029/2006GL025778, 2006.

Worley S. J., S. D. Woodruff, R. W. Reynolds, S. J. Lubker and N. Lott, ICOADS RELEASE 2.1 DATA AND PRODUCTS, *International Journal Climatol.*, *25*, 823 - 842, 2005.

Biogeosciences Discuss., doi:10.5194/bg-2016-228, 2016
Manuscript under review for journal Biogeosciences
Published: 10 June 2016

Figure 1. Annual mean surface height (contour every 6 cm) overlaid on eddy kinetic energy ([$\mathrm{cm^{-2}\,s^{-2}}$], colour), corresponding to: (a) model simulation and (b) *AVISO* observation. Vertical distribution of simulated (c, e) and observed (d, f) mean alongshore velocity [$\mathrm{cm.s^{-1}}$], averaged over 3-6°S (c, d) and at around 12°S (e, f). The observed velocities in Figure 1-d,f were provided by IMARPE and described in detail at Chaigneau et al. (2013).

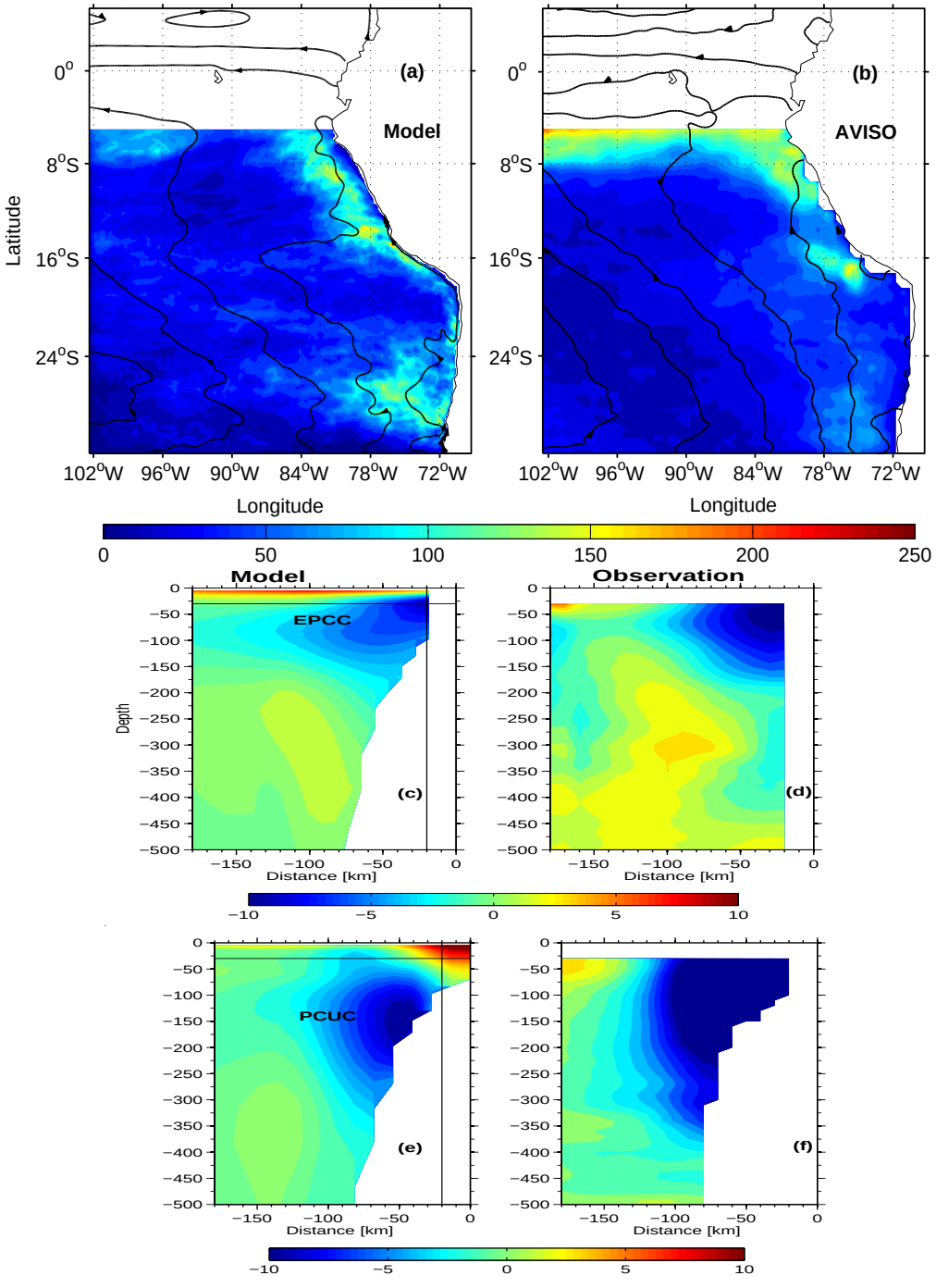

Biogeosciences Discuss., doi:10.5194/bg-2016-228, 2016
Manuscript under review for journal Biogeosciences
Published: 10 June 2016

Figure 2. Sea surface chlorophyll concentration (in $\log_{10}$, [$\mathrm{mg\,m^{-3}}$]) corresponding to (a) model simulation and (b) *MODIS* observation. Oxygen concentration at 400 m depth [$\mu\,\mathrm{mol\,l^{-1}}$] corresponding to (c) model simulation and (d) *CARS* observation.

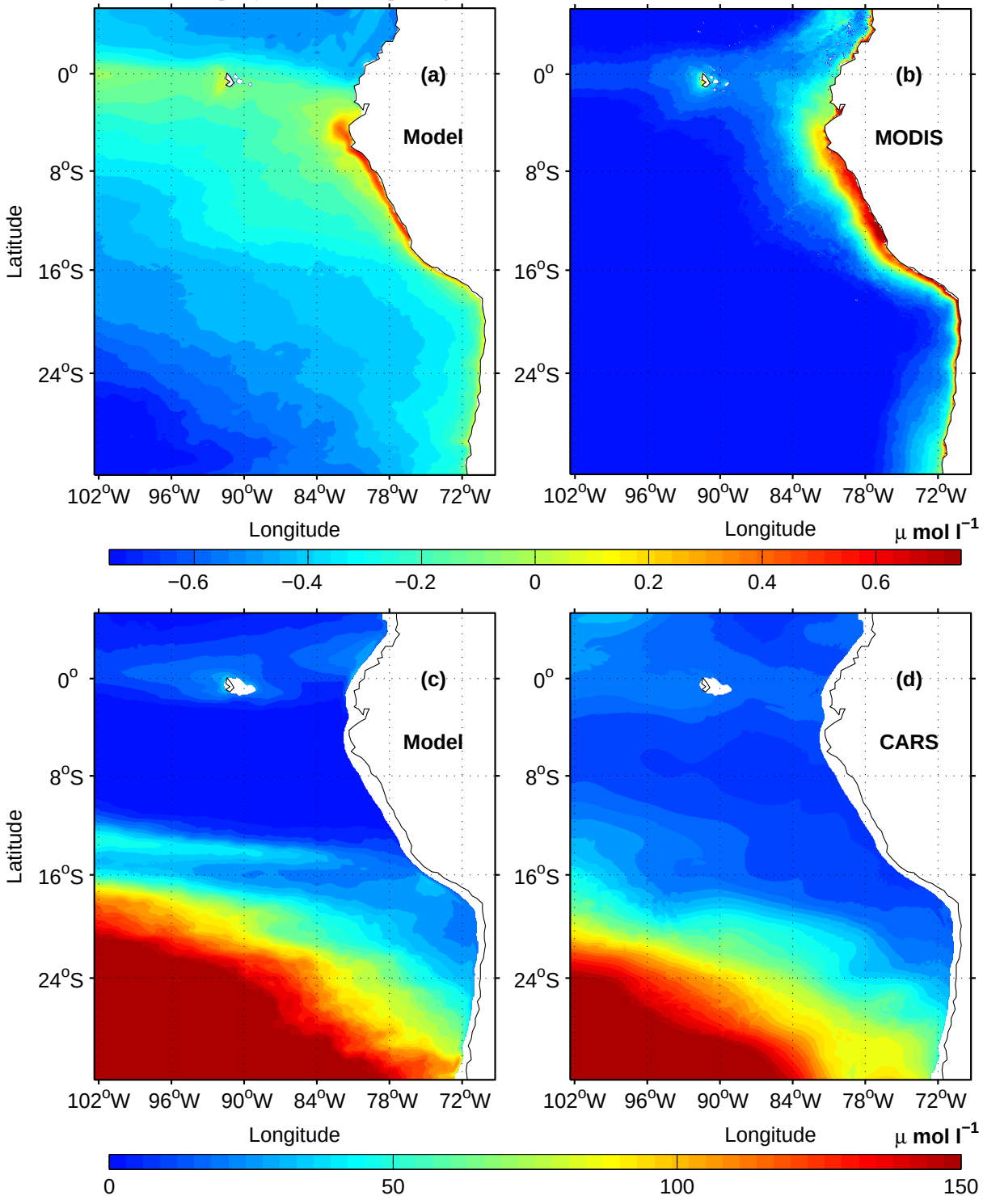

Biogeosciences Discuss., doi:10.5194/bg-2016-228, 2016
Manuscript under review for journal Biogeosciences
Published: 10 June 2016

Biogeosciences Discussions Open Access EGU

Figure 3. Vertical section of oxygen ([µ mol l^{-1}], a), nitrate ([µ mol l^{-1}], b) and nitrite ([µ mol l^{-1}], c) concentrations along 12 °S. Simulated dynamics correspond to climatological December.The observed dynamics is based on measurements from the cruise M91, December 2012. Details about this cruise are described in Czeschel et al. (2015).

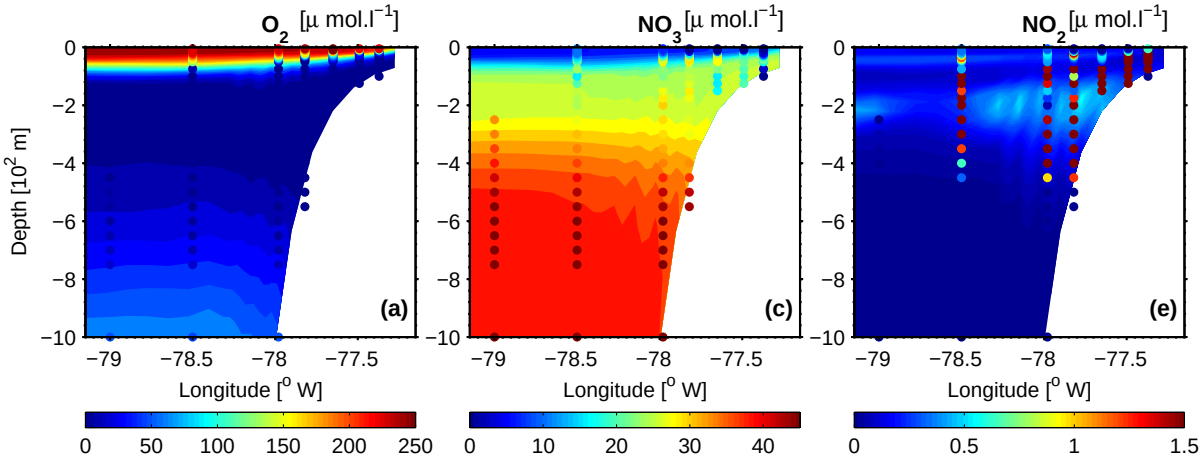

Figure 4. (a) Surface circulation (arrows) overlaid on the surface meridional current [cm s^{-1}], (b) oxygen [µ mol l^{-1}], (c) nitrate [µ mol l^{-1}], (d) nitrite [µ mol l^{-1}] concentrations, (e) meridional velocities [cm s^{-1}], (f) zonal velocities [cm s^{-1}], (g) temperature [°C] and (h) salinity across the eddy A$_{sim}$ center. Nitrate, oxygen, nitrite, temperature, salinity and meridional velocity section around 14.75°S (magenta full line in Fig 4-a). Section for zonal velocity around 77.65°W (magenta dashed line in Fig 4-a). This dynamics corresponds to 21 July model year 30, from now on called identification instant.

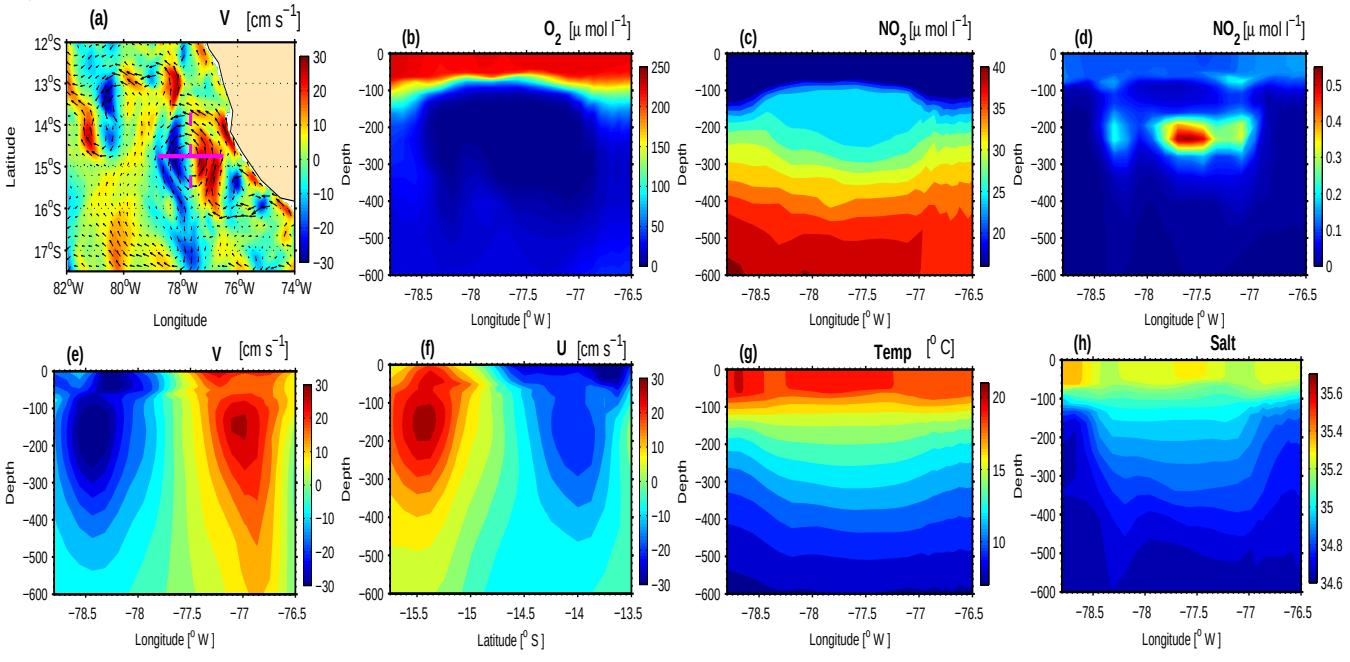

Biogeosciences Discuss., doi:10.5194/bg-2016-228, 2016
Manuscript under review for journal Biogeosciences
Published: 10 June 2016

Biogeosciences Discussions Open Access EGU

Figure 5. (a) Surface circulation (arrows) overlaid on the surface meridional current [$\mathrm{cm\,s^{-1}}$], (b) oxygen [$\mu\,\mathrm{mol\,l^{-1}}$], (c) nitrate [$\mu\,\mathrm{mol\,l^{-1}}$], (d) nitrite [$\mu\,\mathrm{mol\,l^{-1}}$] concentrations, **(e)** meridional velocities [$\mathrm{cm\,s^{-1}}$], (f) zonal velocities [$\mathrm{cm\,s^{-1}}$], (g) temperature [$^{\circ}\mathrm{C}$] and (h) salinity across the eddy B_{sim} center. Nitrate, oxygen, nitrite, temperature, salinity and meridional velocity section around 13.2°S (magenta full line in Fig 5-a). Section for zonal velocity around 85.8°W (magenta dashed line in Fig 5-a). This dynamics corresponds to 27 January model year 28, from now on called identification instant.

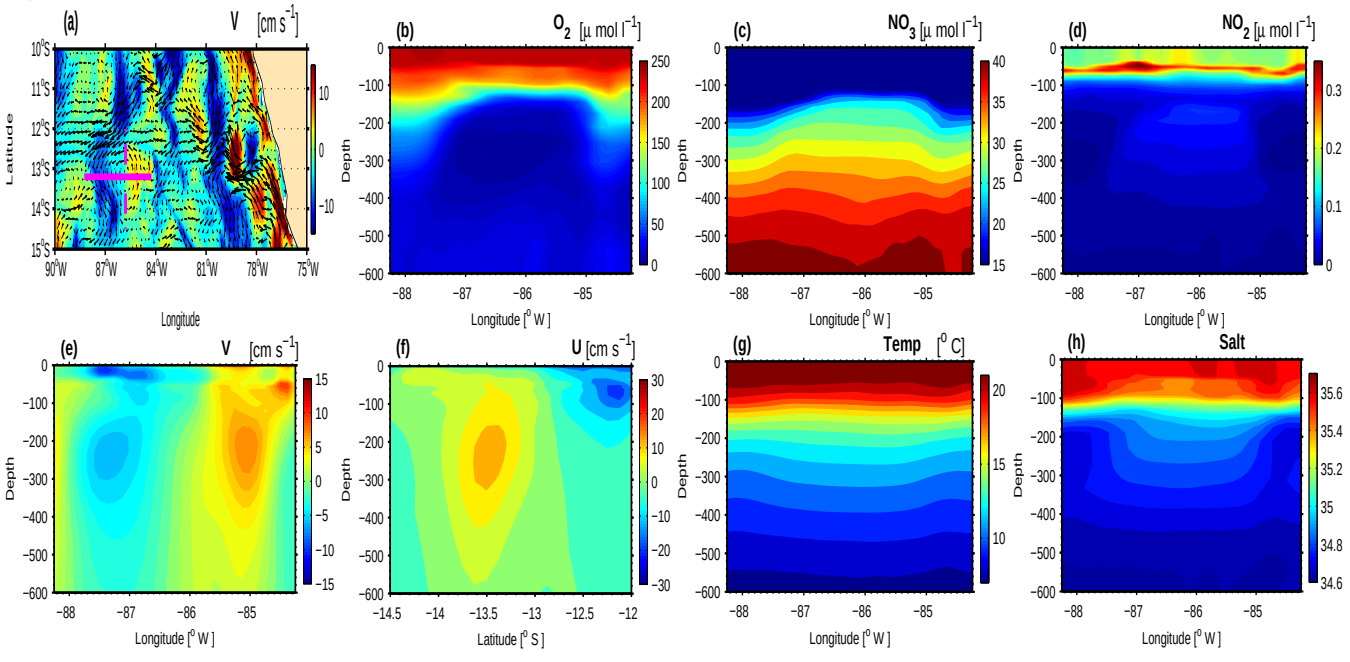

Biogeosciences Discuss., doi:10.5194/bg-2016-228, 2016
Manuscript under review for journal Biogeosciences
Published: 10 June 2016

Biogeosciences Discussions
Open Access
EGU

Figure 6. Eddy A_{sim} vertical structure of: (a) nitrate reduction by denitrification [$\mu\,\mathrm{mol\,l^{-1}}$], (b) nitrate production by nitrification [$\mu\,\mathrm{mol\,l^{-1}}$], (c) nitrate production-reduction difference [$\mu\,\mathrm{mol\,l^{-1}}$], (d) nitrite reduction (nitrification + denitrification + anammox, [$\mu\,\mathrm{mol\,l^{-1}}$]), (e) nitrite production (denitrification + nitrification, [$\mu\,\mathrm{mol\,l^{-1}}$]) and (f) nitrite production-reduction difference [$\mu\,\mathrm{mol\,l^{-1}}$] at the identification instant.

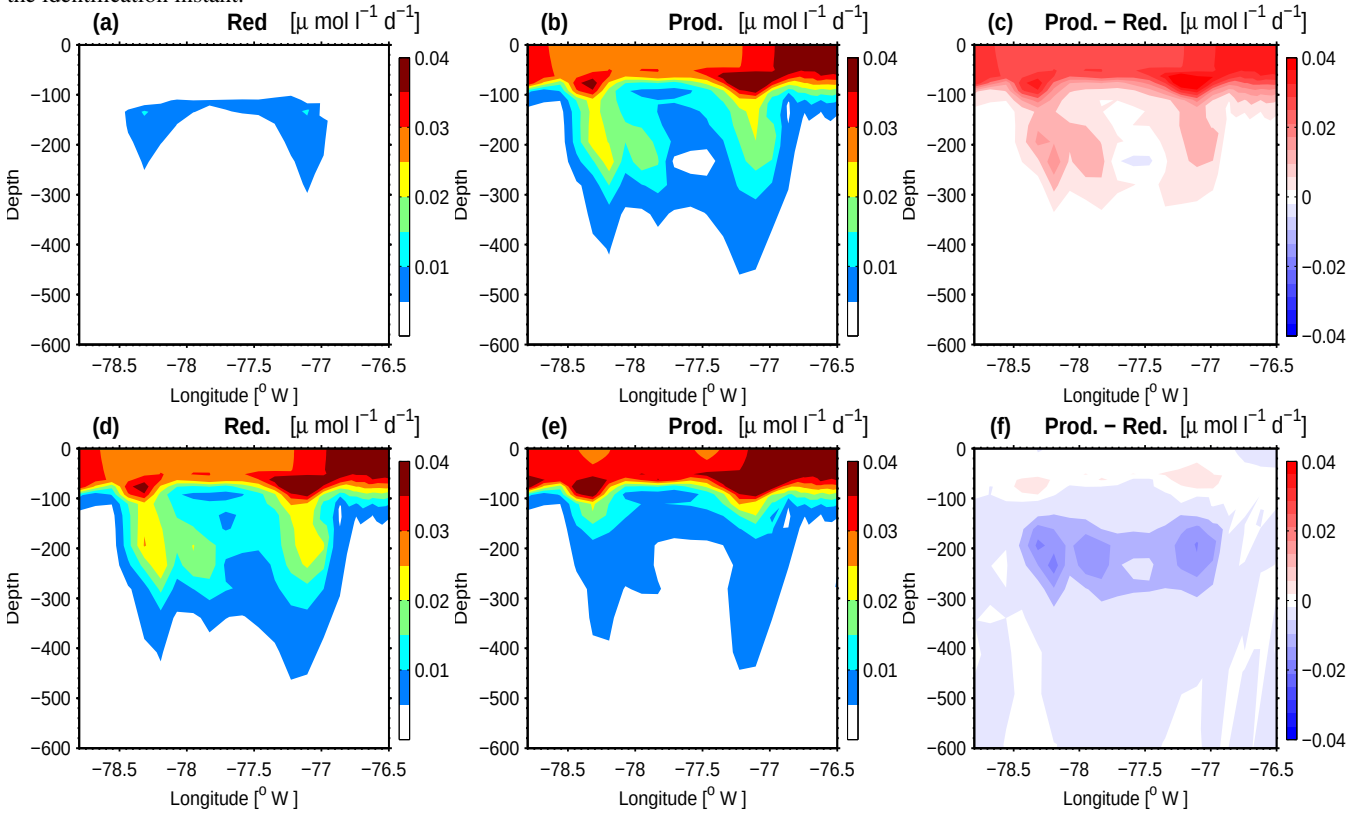

Biogeosciences Discuss., doi:10.5194/bg-2016-228, 2016
Manuscript under review for journal Biogeosciences
Published: 10 June 2016

Biogeosciences Discussions Open Access EGU

Figure 7. (a) Time evolution of cumulative production (black line, [μ mol l^{-1}]), cumulative reduction (cyan line, [μ mol l^{-1}]), production-reduction difference (blue line, [μ mol l^{-1}]) and available nitrate (red line, [μ mol l^{-1}]) within the eddy B_{sim}. (b) The same as (a) but for nitrite. The concentration and fluxes in (a) and (b) correspond to averaged quantities in the upper 400 m depth layer within the eddy structure. Arrow indicates the time where the sections in Figure 4 were made.

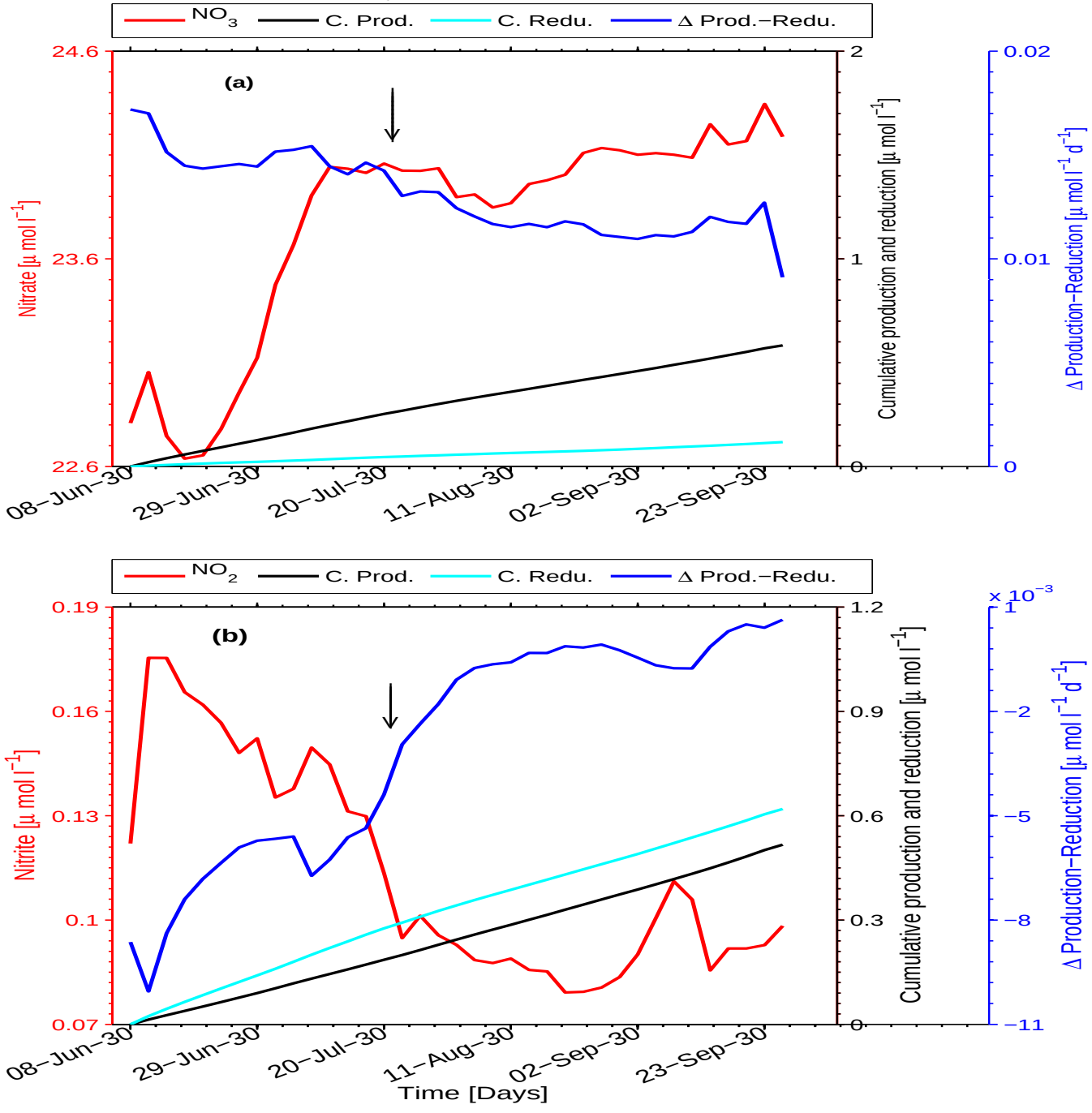

Biogeosciences Discuss., doi:10.5194/bg-2016-228, 2016
Manuscript under review for journal Biogeosciences
Published: 10 June 2016

Biogeosciences Discussions Open Access EGU

Figure 8. Eddy B_{sim} vertical structure of: (a) nitrate reduction by denitrification [$\mu\,\mathrm{mol\,l^{-1}}$], (b) nitrate production by nitrification [$\mu\,\mathrm{mol\,l^{-1}}$], (c) nitrate production-reduction difference [$\mu\,\mathrm{mol\,l^{-1}}$], (d) nitrite reduction (nitrification + denitrification + anammox, [$\mu\,\mathrm{mol\,l^{-1}}$]), (e) nitrite production (denitrification + nitrification, [$\mu\,\mathrm{mol\,l^{-1}}$]) and (f) nitrite production-reduction difference [$\mu\,\mathrm{mol\,l^{-1}}$] at the identification instant.

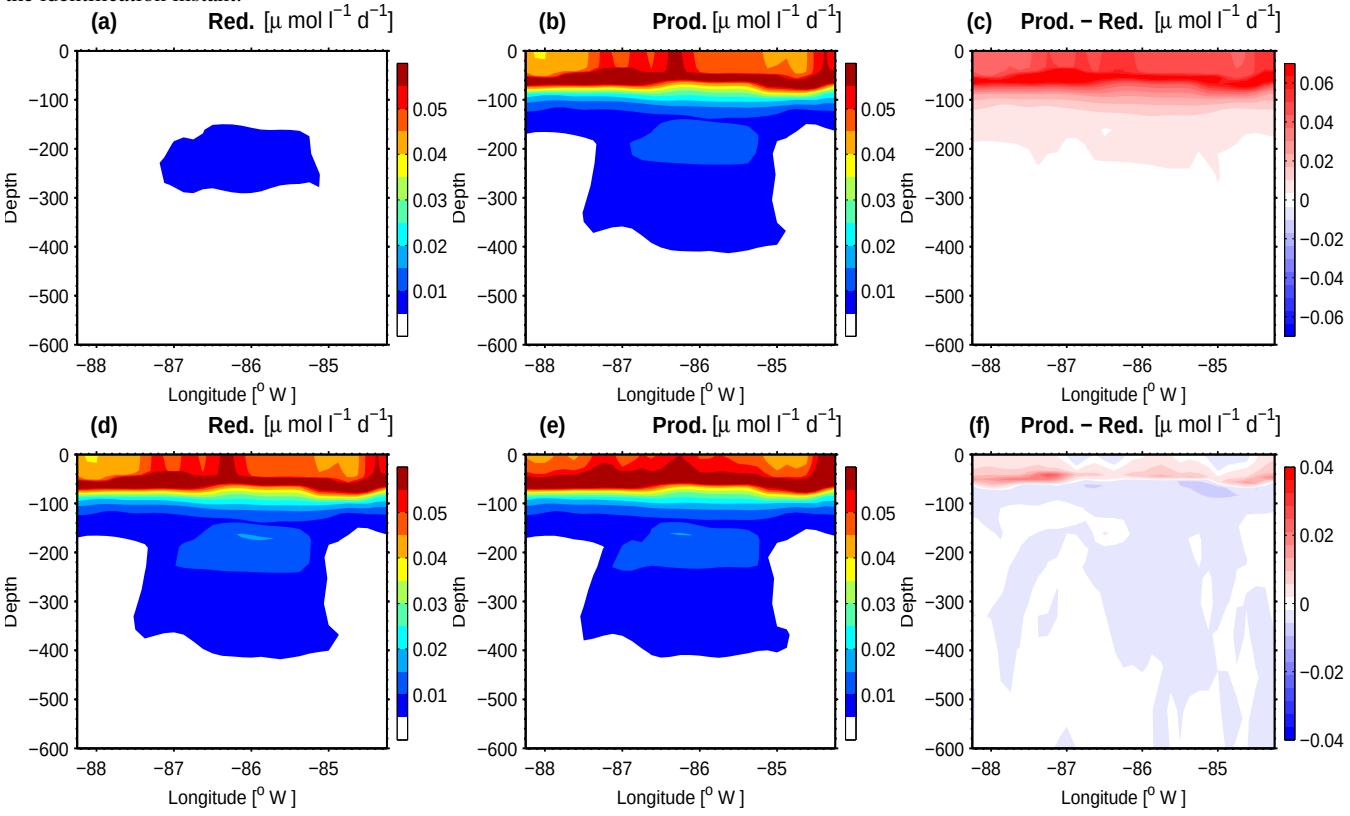

Biogeosciences Discuss., doi:10.5194/bg-2016-228, 2016
Manuscript under review for journal Biogeosciences
Published: 10 June 2016

Biogeosciences Discussions Open Access EGU

Figure 9. (a) Time evolution of cumulative production (black line, [μ mol l^{-1}]), cumulative reduction (cyan line, [μ mol l^{-1}]), production-reduction difference (blue line, [μ mol l^{-1}]) and available nitrate (red line, [μ mol l^{-1}]) within the eddy B_{sim}. (b) The same as (a) but for nitrite. The concentration and fluxes in (a) and (b) correspond to averaged quantities in the upper 400 m depth layer within the eddy structure. Arrow indicates the time where the sections in Figure 5 were made.

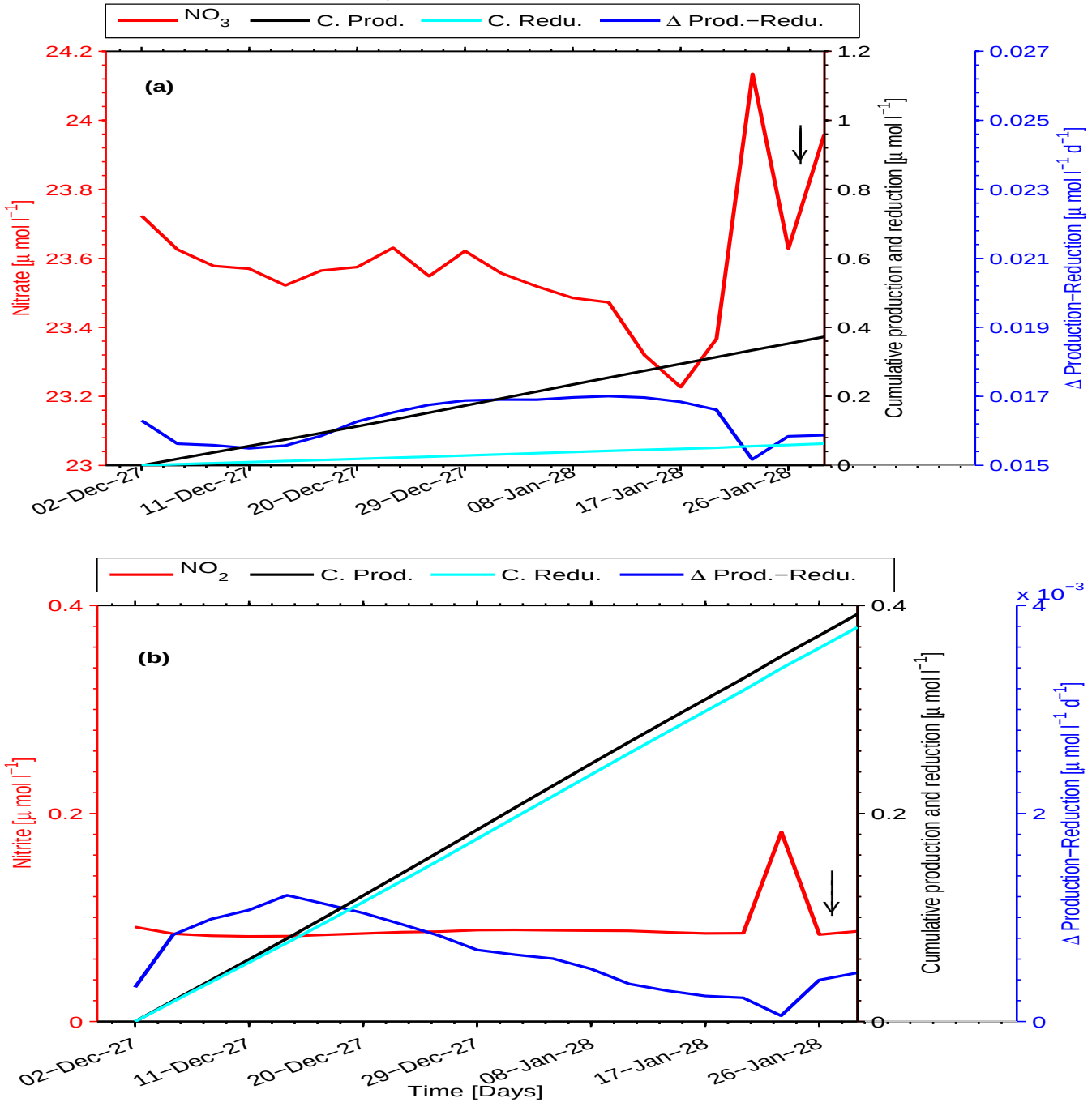

Biogeosciences Discuss., doi:10.5194/bg-2016-228, 2016
Manuscript under review for journal Biogeosciences
Published: 10 June 2016

Biogeosciences Discussions
Open Access
EGU

Figure 10. Spatial distribution of simulated salinity, temperature [°C] and nitrate [μ mol l^{-1}] dynamics around the eddy A_{sim}, corresponding to surface (upper panels), 100m (middle panels) and 250 m depth (bottom panels). Salinity (left panels), temperature (middle-left panels), TS diagram (middle-right panels) and nitrate (right panels). The arrows overlaid on temperature, salinity and nitrate distribution represent the circulation patterns at the eddy's edge. Black and magenta dots in the TS diagram correspond to eddy's water mass properties at the instant after the eddy formation (magenta) and identification instant (black dots). The magenta box in Fig 10-a indicates the region over which TS diagram is calculated.

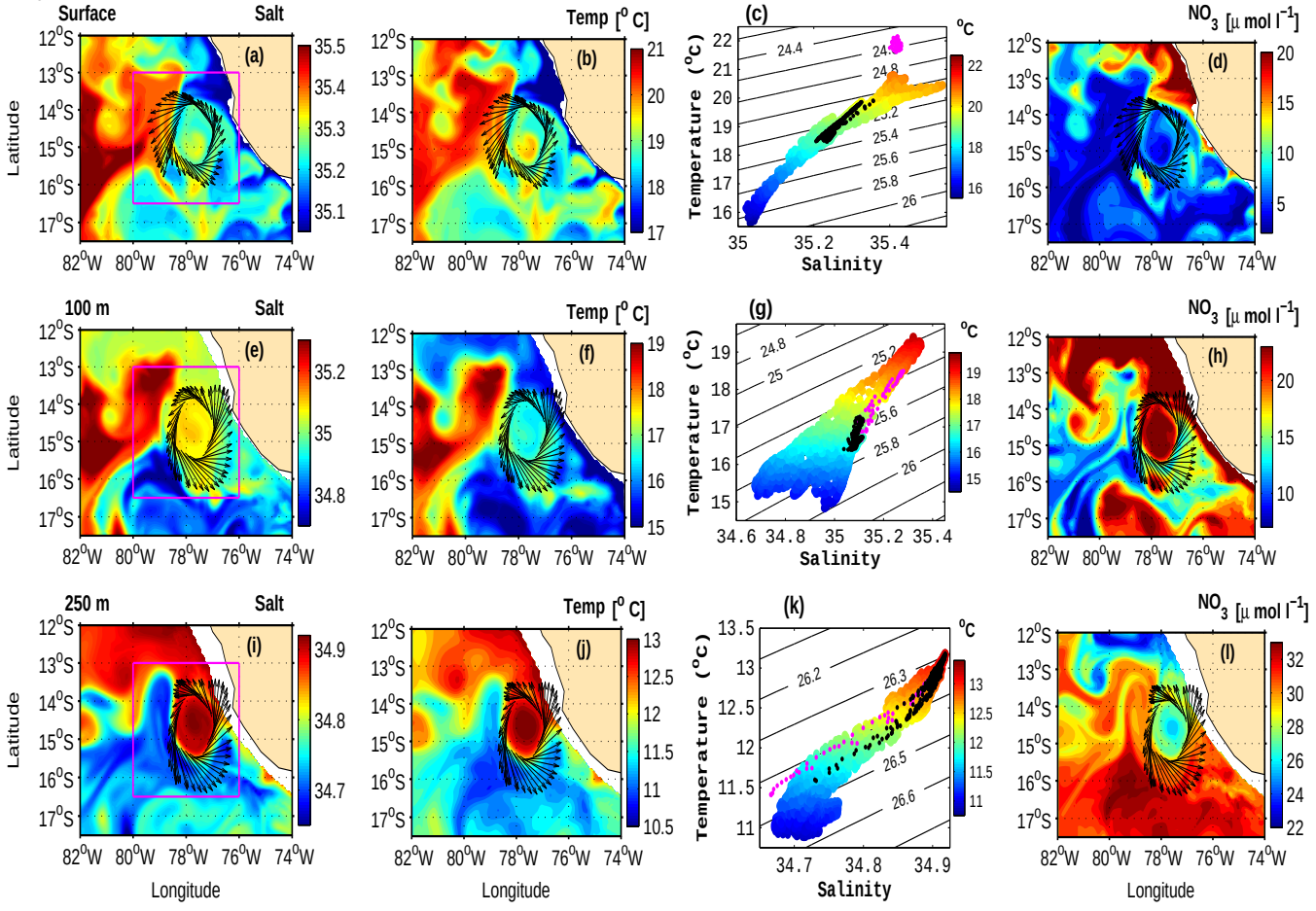

Biogeosciences Discuss., doi:10.5194/bg-2016-228, 2016
Manuscript under review for journal Biogeosciences
Published: 10 June 2016

Biogeosciences Discussions
Open Access
EGU

Figure 11. Spatial distribution of simulated salinity, temperature [°C] and nitrate [μ mol l^{-1}] dynamics around the eddy B_{sim}, corresponding to surface (upper panels), 100m (middle panels) and 250 m depth (bottom panels). Salinity (left panels), temperature (middle-left panels), TS diagram (middle-right panels) and nitrate (right panels). The arrows overlaid on temperature, salinity and nitrate distribution represent the circulation patterns at the eddy's edge. Black and magenta dots in the TS diagram correspond to eddy's water mass properties a month prior to the identification instant (magenta) and identification instant (black dots). The magenta box in Fig 11-a indicates the region over which TS diagram is calculated.